RESEARCH ARTICLE
SOLID EARTH: COMPUTATIONAL GEOPHYSICS

Earth and Planetary Physics
9: 853–860, 2025
doi: 10.26464/epp2025051

First-principles study of the lattice thermal conductivity of $MgSiO_3$ akimotoite in the mantle transition zone

Li Zhang, Zheng Hong, QiLi Chen, Cheng Lu, and KaiHua He*

School of Mathematics and Physics, China University of Geosciences, Wuhan 430074, China

Key Points:

- The thermal conductivities of akimotoite and perovskite of $MgSiO_3$ were estimated, up to 25 GPa and 2500 K, using first-principles calculations; we find that the phase transition of akimotoite → perovskite of $MgSiO_3$ reduces the thermal conductivity.
- The thermal conductivity of $MgSiO_3$ akimotoite exhibits an apparent anisotropy; the azimuthal anisotropy decreases as pressure increases.
- The replacement of 17 mol% Fe for Mg in $MgSiO_3$ akimotoite results in reduction of its thermal conductivity and increase its azimuthal anisotropy.

Citation: Zhang, L., Hong, Z., Chen, Q. L., Lu, C., and He, K. H. (2025). First-principles study of the lattice thermal conductivity of $MgSiO_3$ akimotoite in the mantle transition zone. *Earth Planet. Phys.*, *9*(4), 853–860. http://doi.org/10.26464/epp2025051

Abstract: The lattice thermal conductivity (κ_{latt}) of mantle minerals plays a crucial role in the heat flow and temperature distribution within the Earth. $MgSiO_3$ akimotoite is stable at the bottom of the mantle transition zone; it transitions to $MgSiO_3$ perovskite (MgPv). In this work, we carry out a study of the κ_{latt} of $MgSiO_3$ akimotoite for pressures up to 25 GPa and temperatures up to 2500 K, based on first-principles calculations combined with lattice dynamics theory. At 300 K and 25 GPa, the κ_{latt} of $MgSiO_3$ akimotoite is 37.66 W m^{-1} K^{-1}, larger than that of MgPv (13.46 W m^{-1} K^{-1}), which implies that the phase transition explains the reduction in κ_{latt}. At 300 K, the pressure dependence of κ_{latt} is 0.68 W m^{-1} K^{-1} GPa^{-1}, stronger than that of MgPv (0.48 W m^{-1} K^{-1} GPa^{-1}). The azimuthal anisotropy in κ_{latt} of $MgSiO_3$ akimotoite decreases from 45.5% at 0 GPa to 28.94% at 25 GPa, while the variation trend is opposite to that of MgPv. In $MgSiO_3$ akimotoite, Fe incorporating in the mineral leads to a decrease in κ_{latt} and an increase in azimuthal anisotropy. Along the geotherm, the κ_{latt} of $MgSiO_3$ akimotoite is lower than that of ringwoodite, which would suggest that $MgSiO_3$ akimotoite slows down heat conduction at the bottom of mantle transition zone. These findings are useful for determining the thermal structure of, and understanding heat transfer in, the interior of the Earth.

Keywords: $MgSiO_3$ akimotoite; thermal conductivity; phase transition; anisotropy; first-principles calculations

1. Introduction

Lattice thermal conductivity, which dictates the heat transfer properties of materials, is a fundamental physical quantity and is essential for understanding the dynamics and thermal evolution of the Earth's interior (Gubbins et al., 2007; Lay et al., 2008; Chao KH and Hsieh, 2019). The mantle transition zone (MTZ) is a part of the mantle located at depths of 410–660 km. It forms a link between the upper and lower mantle, and is an important place to study mantle convection and thermal cycling. Complex phase transitions are known to exist in the MTZ. Some of them are known to change the physical properties of mantle minerals to a large extent, such as their elasticity (Liu M and Yund, 1995; Carpenter and Zhang ZY, 2011; Núñez-Valdez et al., 2011, 2012, 2013), thermodynamic properties (Suzuki et al., 1979a, 1980b; Meng Y et al., 1993; Li L et al., 2007), thermal conductivity (Hofmeister, 2001; Xu YS et al., 2004), and seismic wave velocity (Ringwood, 1975; Jackson, 1983; Tauzin et al., 2008; Kawai and Tsuchiya, 2009; Weidner and Li L, 2010; Yu YG et al., 2011; Hernández et al., 2015; Cottaar and Deuss, 2016; He J et al., 2022). The phase transition of olivine → wadsleyite and wadsleyite → ringwoodite have been shown to account for the seismic discontinuities observed at 410 km and 520 km; meanwhile, κ_{latt} increases contemporaneously with these phase transitions (Yang S et al., 2023). At a depth of 660 km, which marks the beginning of the lower mantle, ringwoodite is expected to decompose into bridgmanite and ferropericlase (Ito and Takahashi, 1989).

Other researches have revealed that $MgSiO_3$ akimotoite remains stable at pressures of 18–25 GPa, implying the existence of $MgSiO_3$ akimotoite with an ilmenite structure at the bottom of the MTZ (Wang YB et al., 2004; Zhang YG et al., 2005). The elasticity and wave velocity of $MgSiO_3$ akimotoite have been subject to comprehensive studies (Li L et al., 2009; Siersch et al., 2021; Zhao YJ et al., 2022). Zhao YJ et al. (2022) derived the seismic velocity and density of pyrolite using a model that takes into account the

First author: L. Zhang, zzhangli@cug.edu.cn
Correspondence to: K. H. He, khhe@cug.edu.cn
Received 22 NOV 2024; Accepted 18 MAR 2025.
First Published online 19 MAY 2025.

distribution of lateral temperature heterogeneities (i.e., lateral, low-temperature anomalies that can lead to the presence of $MgSiO_3$ akimotoite). Their results match well with 1D seismological models such as PREM (Dziewonski and Anderson, 1981) and AK135 (Kennett et al., 1995). The $R\bar{3}$ space-group structure of $MgSiO_3$ akimotoite has strong elastic anisotropy resulting from its lattice preferred orientation (LPO), a feature that can be utilized to unveil seismic anisotropies that occur in the vicinity of the subducted plate region in the lower part of the MTZ (Li L et al., 2009; Hao SQ et al., 2019; Siersch et al., 2021; Guan LL et al., 2022; Zhao YJ et al., 2022). In turn, κ_{latt} is related to structural and elastic properties, and it has been hypothesized that the κ_{latt} of $MgSiO_3$ akimotoite is also anisotropic. Such anisotropy will affect the heat flow and temperature distribution in the Earth's interior; thus, determining it precisely will further assist us in exploring the thermal evolution of the mantle while simultaneously enhancing our comprehension of the thermal structure of the Earth's interior.

$MgSiO_3$ akimotoite transitions into MgPv at relatively low temperatures in subducted slabs at mantle depths of 700–750 km. Chanyshev et al. (2022) reported that the $MgSiO_3$ akimotoite → MgPv transition boundary has an extremely steep negative slope, especially at low temperatures, which can explain the significant collapse of the upper and lower mantle boundaries in subducted plate regions. Meanwhile, this phase transition, together with the post-spinel transition, accounts for the double seismic discontinuities at 660 km and 740 km. Evidence of seismic discontinuities and the anisotropy of $MgSiO_3$ akimotoite also have a close connection with κ_{latt}. However, attempts at experimental measurements of the mineral's κ_{latt} at high temperatures and pressures have remained elusive. So far, knowledge of κ_{latt} values of $MgSiO_3$ akimotoite is unclear, limiting our knowledge of the thermal structure of the transition zone.

In this study, we focus on obtaining κ_{latt} values by solving the Boltzmann transport equation (BTE), which has been confirmed to be reliable (Dekura and Tsuchiya, 2017, 2019; Ouyang YL et al., 2022; Wang D et al., 2023). First, the κ_{latt} of $MgSiO_3$ akimotoite and MgPv are calculated based on first principles (Section 2). Then, the differences between $MgSiO_3$ akimotoite and MgPv, as well as their pressure and temperature dependence and the anisotropy of κ_{latt}, are discussed (Section 3). We conclude our paper in Section 4.

2. Calculational Details

Both the structural optimization and physical properties calculations of $MgSiO_3$ akimotoite were completed with the Vienna Ab-initio Simulation Package (VASP) based on density functional theory (DFT) (Kresse and Furthmüller, 1996; Kresse and Joubert, 1999; Lu C and Chen CF, 2021). The exchange potential is described using the generalized gradient approximation, in the framework of DFT, with projection augmented waves (Hohenberg and Kohn, 1964; Kohn and Sham, 1965; Blöchl, 1994). Convergence tests were performed to determine the cutoff energy, which was set to 700 eV (Figure S1), and K-points were generated using the Monkhorst–Pack approach (Monkhorst and Pack, 1976) with a 6 × 6 × 2 grid. The convergence threshold was set to 1 × 10^{-8} eV $cell^{-1}$ for the total energy and 10^{-3} eV $Å^{-1}$ for the atomic force.

The phonon dispersion, second-order interatomic force constants (IFCs), and thermodynamic parameters were calculated based on the quasi-harmonic approximation (QHA) using the finite displacement method in the PHONOPY software (Togo and Tanaka, 2015). We computed the thermal expansion (Figure S2) to verify the applicability of the QHA. A 2 × 2 × 1 supercell containing 120 atoms was chosen and 3 × 3 × 2 K-points were used. The other parameters were set up in exactly the same way as they were for the structural optimization.

The BTE was solved after the third-order force constants were obtained with the ShengBTE package (Li W et al., 2014). To compute the third-order IFCs, the cut-off range for atomic interactions was set at 4.0 Å; the corresponding convergence test is shown in Figure S3. The trial displacements of atoms were chosen to be 0.01 Å for the calculations of third-order IFCs. The details and parameters used in the calculations were the same as those for calculating the second-order IFCs. Due to the sensitivity of κ_{latt} to the value of the q-point, we experimented with different values and eventually found that a 13 × 13 × 7 grid provided good convergence (Table S1). In general, the κ_{latt} at different temperatures can be expressed as the sum of the contributions of all phonon modes, λ, under the branching index, p, and wave vector, q (Liang T et al., 2018):

$$\kappa_{latt}^{ij} = \frac{1}{3N\Omega}\sum_{\lambda} C_{\lambda} v_{\lambda i} v_{\lambda j} \tau_{\lambda}, \tag{1}$$

where N is the atomic number, Ω is the volume, C is the heat capacity, and v and τ represent the group velocity and the phonon lifetime, respectively, which are calculated via DFT. In order to discuss the relation between elastic constants and thermal conductivity, the elastic constants were also calculated by local-density approximation (LDA). For considering the effect of Fe, one Fe atom substitutes the Mg atom in a 2 × 2 × 1 (120 atoms) $MgSiO_3$ akimotoite supercell, as well as for MgPv, a 2 × 2 × 2 (160 atoms) supercell is used. Under the condition of the mantle transition zone, the high spin state of ferrous iron was selected.

3. Result and Discussion

3.1 κ_{latt} of $MgSiO_3$ Akimotoite

Figure 1 shows how κ_{latt} varies under high temperature and high pressure for Fe-free and Fe-bearing akimotoite; results for MgPv are also shown. Under ambient conditions, κ_{latt} of $MgSiO_3$ akimotoite and of MgPv are 20.67 and 12.9 W m^{-1} K^{-1}, respectively, which implies that the phase transition of $MgSiO_3$ akimotoite → MgPv leads to a reduction in κ_{latt}. For MgPv, the calculated value of 12.9 W m^{-1} K^{-1} agrees well with the previous reports of Ghaderi et al. (2017) and Zhang Z and Wentzcovitch (2021), but it is nearly twice as large as that measured by Ohta et al. (2012), who used a diamond anvil cell with a newly developed technique. Two main reasons for the apparent discrepancy have been proposed: (1) the calculations are mainly based on ideal crystals and do not take into account the presence of defects in the experimental samples, which impacts the scattering rate (Haigis et al., 2012; Imada et al., 2014); and (2) the experimental measurements of κ_{latt} are based on polycrystalline samples, which leads to an underestimation of the single-crystal κ_{latt} due to the effects of polycrystalline scattering

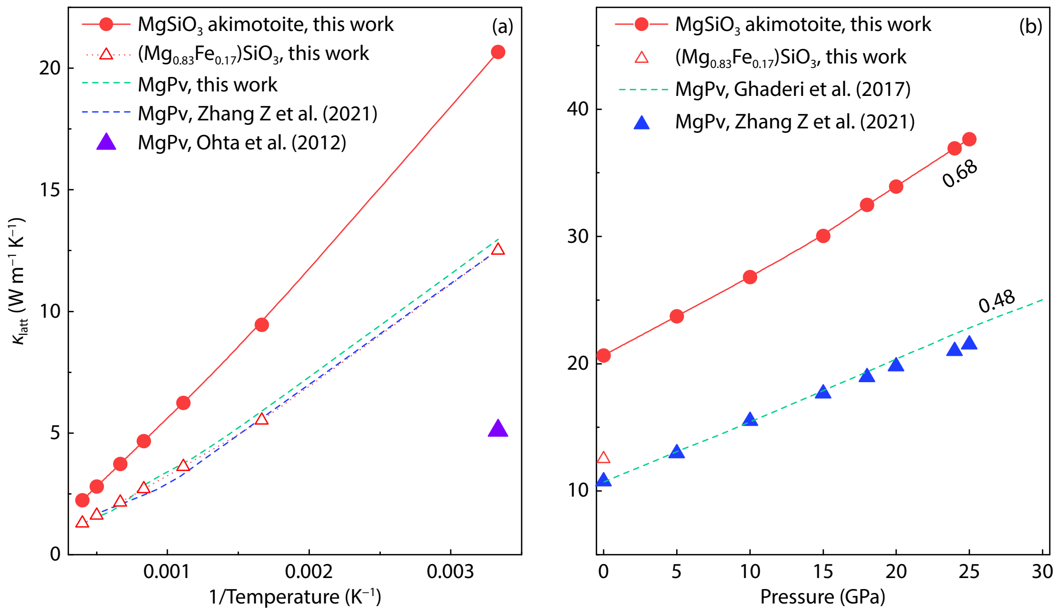

Figure 1. (a) Temperature dependence of κ_{latt} of $MgSiO_3$ akimotoite, $(Mg_{0.83}Fe_{0.17})SiO_3$ and MgPv at 0 GPa; (b) pressure dependence of κ_{latt} of $MgSiO_3$ akimotoite, $(Mg_{0.83}Fe_{0.17})SiO_3$ and MgPv at 300 K.

(Ohta et al., 2017).

At 300 K, the κ_{latt} of $MgSiO_3$ akimotoite increases from 20.67 to 37.66 W m^{-1} K^{-1} as the pressure increases from 0 GPa to 25 GPa, and it decreases to 3.76 W m^{-1} K^{-1} as the temperature increases to 2500 K. The temperature dependence of κ_{latt} can be expressed as $T^{-1.04}$ and $T^{-1.02}$ for $MgSiO_3$ akimotoite and MgPv, respectively, both of which are close to the typical semiconductor relation of T^{-1}.

κ_{latt} increases almost linearly under the effects of pressure; the slope of $MgSiO_3$ akimotoite is 0.68 W m^{-1} K^{-1} GPa^{-1}, which is larger than that of MgPv (0.48 W m^{-1} K^{-1} GPa^{-1}). In the next paragraph, we attempt to explore the factors influencing the reduction in κ_{latt} that result from the phase transition of $MgSiO_3$ akimotoite → MgPv.

The cumulative κ_{latt} of $MgSiO_3$ akimotoite and MgPv at 25 GPa and 300 K is shown in Figure 2. It can be seen that the κ_{latt} increases rapidly in the low-frequency range and gradually stabilizes, which implies that the κ_{latt} of $MgSiO_3$ akimotoite and MgPv are mainly determined by phonons with frequencies below 145 rad ps^{-1} and 125 rad ps^{-1}, respectively. The volumes of $MgSiO_3$ akimotoite and MgPv (20 atoms) are 170.95 and 146.39 Å^3, respectively. $MgSiO_3$ akimotoite has a larger volume, reducing its κ_{latt}, which is the opposite of the actual trend of κ_{latt}. As seen in Equation (1), κ_{latt} is determined primarily by heat capacity, phonon lifetime, and group velocity. The heat capacity remains constant at higher temperature and does not change, so it has a negligible effect on κ_{latt}. Therefore, we have concentrated on the effects of phonon lifetime and group velocity.

Figure 3 illustrates how the anharmonic scattering rate (the reciprocal of the phonon lifetime) and group velocity vary at different temperatures and pressures. Obviously, the anharmonic scattering rate of MgPv is stronger than that of $MgSiO_3$ akimotoite, which implies that $MgSiO_3$ akimotoite has a longer phonon lifetime. The

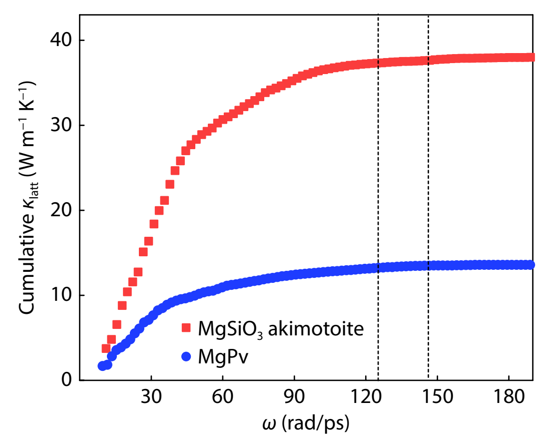

Figure 2. Cumulative κ_{latt} as a function of frequency at 25 GPa and 300 K.

group velocity of $MgSiO_3$ akimotoite is higher than that of MgPv. Therefore, the variations in phonon lifetime and group velocity support the conclusion that the reduction in κ_{latt} results from the phase transition of $MgSiO_3$ akimotoite → MgPv. Furthermore, it can be seen that the anharmonic scattering rate of $MgSiO_3$ akimotoite and MgPv increases as the temperature increases, which leads to a decrease in κ_{latt}. In general, the anharmonic scattering rate is determined by the third-order IFCs and the weighted phase space. At 25 GPa, the maximum third-order IFC elements for $MgSiO_3$ akimotoite and MgPv are 63.8 eV Å^{-3} and 63 eV Å^{-3}, respectively. The small difference in the third-order IFCs has a negligible effect on κ_{latt}.

Furthermore, we introduced the weighted phase space to verify the three-phonon scattering process (Li W and Mingo, 2014). The total phase space of the three-phonon scattering process consists of two separate scattering channels: an absorption process (ω^+) and an emission process (ω^-). It can be observed that the weighted phase space increases with temperature increase, which

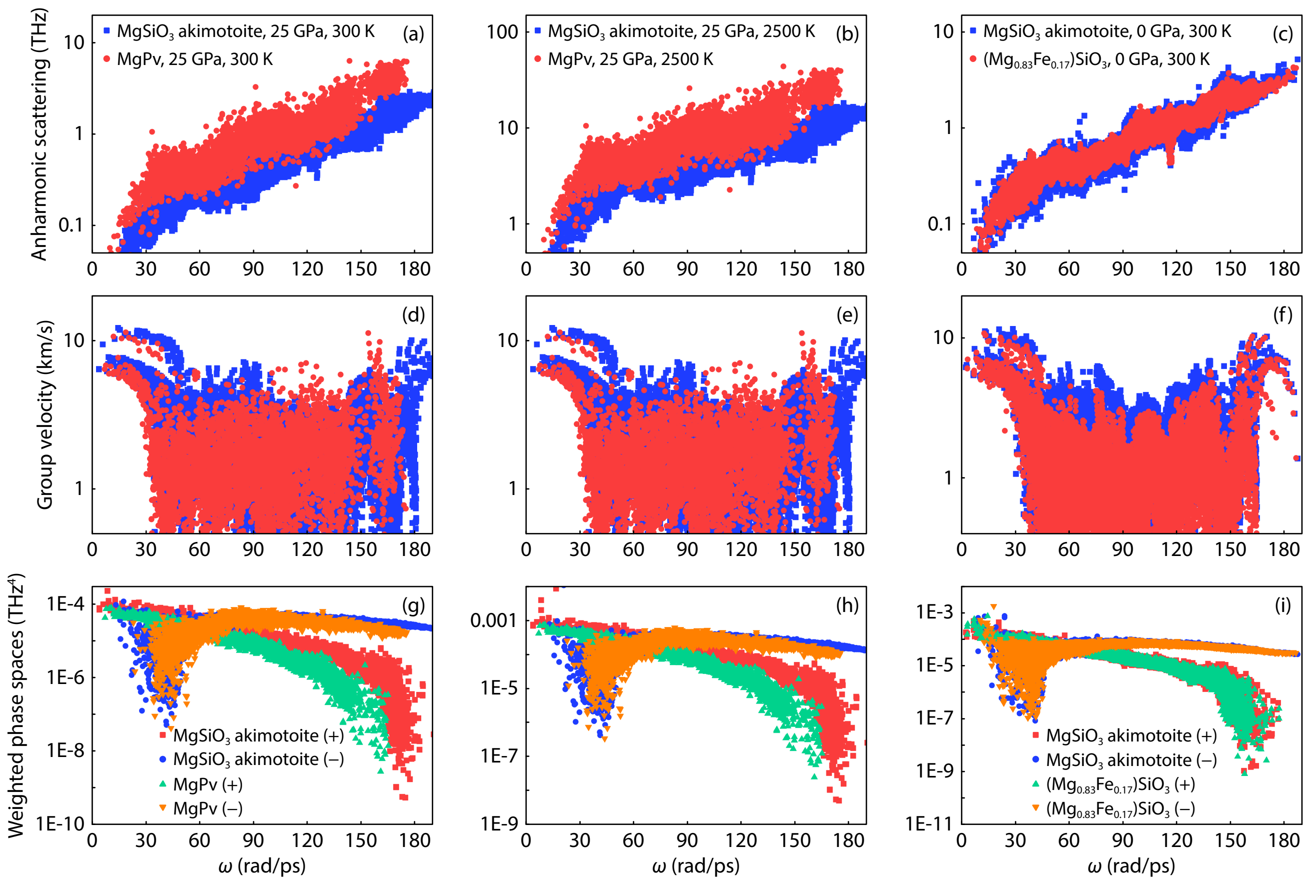

Figure 3. Anharmonic scattering rate (a, b), group velocity (d, e), and weighted phase space (g, h) of $MgSiO_3$ akimotoite and MgPv at 25 GPa and 300 K, 2500 K. Comparison of the anharmonic scattering rate (c), group velocity (f) and weighted phase space (i) of Fe-free and Fe-bearing akimotoite at 0 GPa and 300 K.

is consistent with the variation of the scattering rate with temperature. Therefore, the variations of the weighted phase space determine the change of scattering rates, which in turn affects κ_{latt}.

3.2 The Anisotropy of κ_{latt} for $MgSiO_3$ Akimotoite

The elastic constants of $MgSiO_3$ akimotoite and ringwoodite were estimated using the Voigt–Reuss–Hill scheme; we find that $MgSiO_3$ akimotoite shows stronger anisotropy than that of ringwoodite. This property can be reasonably extrapolated to determine the seismic characteristics at the bottom of the MTZ (Zhang YG et al., 2005). Figure 4a presents the variation of κ_{latt} at 0 GPa along different directions for Fe-free and Fe-bearing akimotoite and for MgPv. The κ_{latt} of $MgSiO_3$ akimotoite along different directions exhibits the relationship of $\kappa_a = \kappa_b > \kappa_c$, which is in accordance with the relationship of the elastic constants, $C_{11} = C_{22} > C_{33}$ (Table 1) (Weidner and Ito, 1985; Zhao YJ et al., 2022). The amplitude of the κ_{latt} in this study is represented by the arithmetic mean of the principal components κ_a, κ_b and κ_c, given by $\kappa_{latt} = (\kappa_a + \kappa_b + \kappa_c)/3$. It can be seen that κ_{latt} decreases sharply as the temperature increases in all three directions. The κ_a and κ_b of $MgSiO_3$ akimotoite is 23.81 W m^{-1} K^{-1} at 0 GPa and 300 K, which is roughly 1.7 times that of κ_c (14.39 W m^{-1} K^{-1}). Moreover, the reduced magnitudes of κ_a and κ_b are greater than for κ_c. Under the same conditions, MgPv presents ratios of $\kappa_a/\kappa_b = 1.13$ and $\kappa_c/\kappa_b = 1.36$. The κ_{latt} in each direction tends to increase almost linearly as the pressure increases; the fitted equations are shown in Figure 4b. $MgSiO_3$ akimotoite has its strongest pressure dependence along the *a*-axis, whereas that of MgPv is along the *c*-axis. The azimuthal anisotropy is described by $A = (\kappa_{\max} - \kappa_{\min})/\kappa_{mean}$; the variation with temperature at 0 GPa is illustrated in Figure 5. The azimuthal anisotropy of $MgSiO_3$ akimotoite is greater than that of MgPv, and has a slight decrease with increasing temperature. Under ambient conditions, the azimuthal anisotropy of $MgSiO_3$ akimotoite is A = 45.5% at 0 GPa and 28.94% at 25 GPa; this indicates that the mineral's azimuthal anisotropy decreases as the pressure increases. This extent of anisotropic variation is comparable to that of the upper mantle mineral olivine (Osako et al., 2004). However, for MgPv we find A = 30.79% at 0 GPa and 35.75% at 25 GPa, a variation that is in accordance with the calculations of Ghaderi et al. (2017). The azimuthal anisotropy of $MgSiO_3$ akimotoite exhibits a stronger pressure dependence than that of MgPv, but a relatively weaker temperature response.

3.3 Effect of Fe on κ_{latt}

Pertermann and Hofmeister (2006) demonstrated that minor elements have a tremendous impact on the κ_{latt} of mantle minerals. In particular, the effect of Fe on the κ_{latt} of minerals has been continuously explored; Fe incorporation has been found to lead to a decrease in κ_{latt} (Hsieh et al., 2017; Okuda et al., 2019; Wang D et al., 2023). Accordingly, we research the effect of Fe doping on the κ_{latt} of $MgSiO_3$ akimotoite. At ambient temperature, we find

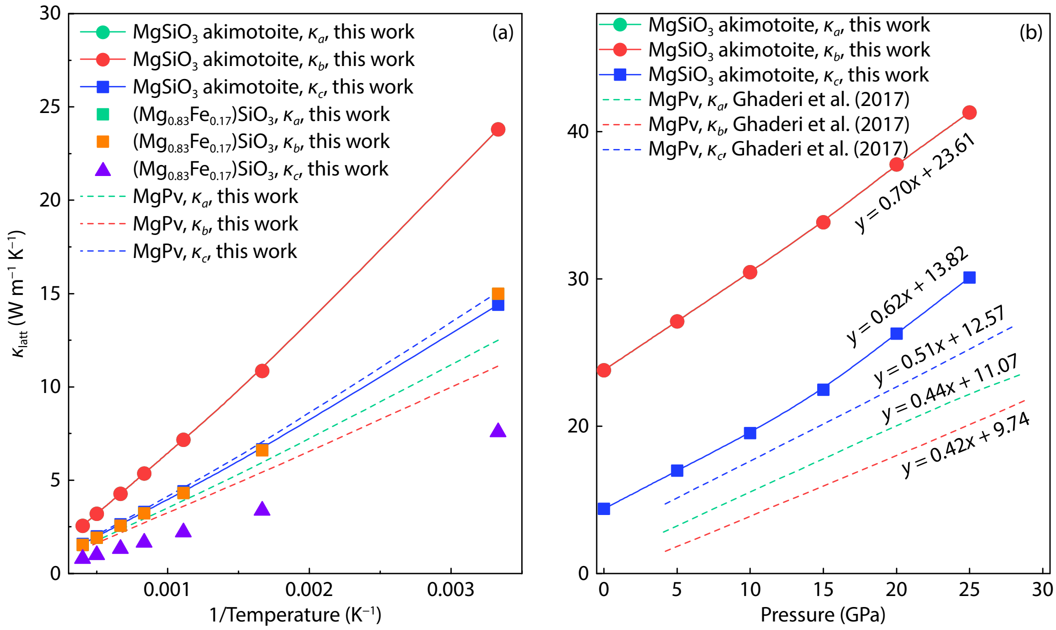

Figure 4. Variation of κ_{latt} with temperature (a) and pressure (b) along different directions for Fe-free and Fe-bearing akimotoite and MgPv.

Table 1. κ_{latt} and elastic constants of $MgSiO_3$ akimotoite along different directions.

	κ_{latt} (W m^{-1} K^{-1})	Elastic constants (GPa)	
$MgSiO_3$ akimotoite	κ_a = 23.81	C_{11} = 475.3	C_{11} = 472 (Zhao YJ et al., 2022)
	κ_b = 23.81	C_{22} = 475.3	C_{22} = 472 (Zhao YJ et al., 2022)
	κ_c = 14.39	C_{22} = 396.2	C_{33} = 382 (Zhao YJ et al., 2022)

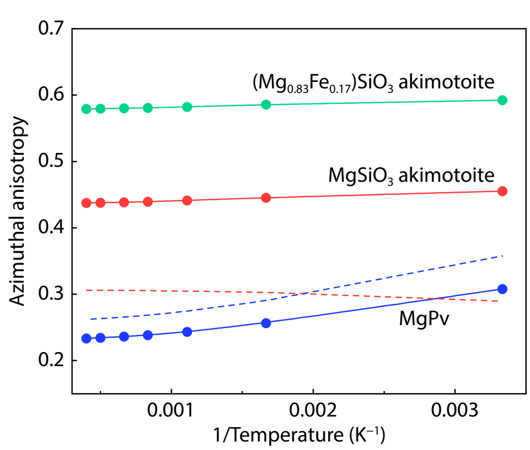

Figure 5. Temperature dependence of azimuthal anisotropy of the κ_{latt} of Fe-free and Fe-bearing akimotoite and MgPv: at 0 GPa (solid lines); at 25 GPa (dashed lines).

that the κ_{latt} of $MgSiO_3$ akimotoite decreased by ~39%, and this change is the same as the presence of Fe in the lower mantle reduces the κ_{latt} of MgPv and $MgSiO_3$ post-perovskite (MgPPv) (Wang D et al., 2023). As shown in the Figure 4, the higher anharmonic scattering rate and lower group velocity plausibly account for the reduced κ_{latt} due to Fe impurities. Meanwhile, we notice that the κ_{latt} of Fe-bearing akimotoite along different directions are smaller than those in the corresponding directions of Fe-free akimotoite (Figure 4). For the azimuthal anisotropy, Fe-bearing akimotoite is greater than that of Fe-free akimotoite (Figure 5), which shows that the incorporation of Fe increases the azimuthal anisotropy. In addition, the variation of anisotropy is consistent with the observation that greater inclusion of iron increases the elastic anisotropy of $MgSiO_3$ akimotoite (Zhao YJ et al., 2022).

3.4 κ_{latt} of $MgSiO_3$ Akimotoite in Geothermal Conditions

The temperature and pressure in the Earth's interior increase with depth. As demonstrated in Figure 6, we predicted the variation of κ_{latt} along the geotherms for olivine, wadsleyite, ringwoodite, $MgSiO_3$ akimotoite, and MgPv. The phase transitions of olivine → wadsleyite → ringwoodite are accompanied by an increase in κ_{latt}, while the $MgSiO_3$ akimotoite → MgPv transition decreases κ_{latt}. Heat flow, an important parameter characterizing the thermal state of the Earth's interior, is affected by the κ_{latt} of the minerals at the corresponding depths, and its behavior can help us understand the distribution of temperature inhomogeneities in the mantle.

The LPO of $MgSiO_3$ akimotoite also impacts heat flux due to the crystallographic orientation dependence of κ_{latt}. Combining Fourier's law for heat flux, $q = \kappa_{latt}\dfrac{\Delta T}{\Delta z}$, and then solving for the heat flow value at a 660 km depth by substituting the κ_{latt} value of 4.94 W m^{-1} K^{-1} for $MgSiO_3$ akimotoite (calculated at 660 km and r = 5711 km, $\Delta T/\Delta z$ = 0.43), (Yang DP et al., 2017; Liu J et al., 2019) we obtain $Q_{660} = 4\pi r^2 q = 0.87$ TW, which is larger than the heat flow values at 410 km (0.43 TW) and 520 km (0.75 TW) (Yang S et

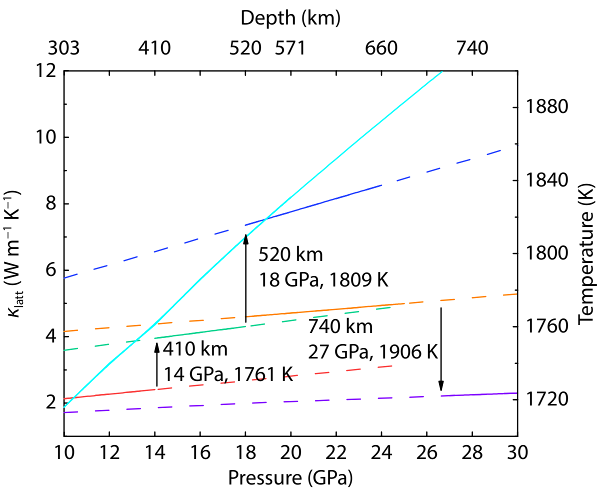

Figure 6. Extrapolated κ_{latt} of olivine (red line) (Yang S et al., 2023), wadsleyite (green line) (Yang S et al., 2023), ringwoodite (blue line) (Yang S et al., 2023), $MgSiO_3$ akimotoite (orange line), MgPv (purple line) (Zhang Z and Wentzcovitch, 2021) along the geotherm. The cyan line represents the geotherm.

al., 2023). Meanwhile, we find that the heat flow at 660 km (Q_{660}) corresponds to ~15–29% of the heat flow at the core–mantle boundary (3–6 TW) (Weidner and Ito, 1985; Dekura et al., 2013). However, this estimate is based on the current model and assumptions; further data and analysis are needed to confirm the result. Understanding these heat flow variations allows us to develop a better understanding of the temperature distribution, and provides insights for characterizing the heat flow, in the Earth's interior.

4. Conclusions

In summary, we determined the κ_{latt} of $MgSiO_3$ akimotoite at high temperature and pressure, up to 25 GPa and 2500 K, respectively, using first-principles calculations combined with the anharmonic lattice dynamics approach. κ_{latt} has a negative dependence on temperature and increases as the pressure increases. Under ambient conditions, the calculated κ_{latt} of $MgSiO_3$ akimotoite is 20.67 W m^{-1} K^{-1}, which is larger than that of MgPv, suggesting that the transition of $MgSiO_3$ akimotoite → MgPv results in a reduction of κ_{latt} due to the lower anharmonic scattering rate and higher group velocity of $MgSiO_3$ akimotoite. Moreover, we observe ~39% reduction in the κ_{latt} of $MgSiO_3$ akimotoite under ambient conditions, which we ascribe to the presence of 17 mol% Fe. Furthermore, the anisotropy of κ_{latt} increases with increasing pressure, displaying a sharp pressure dependence in the *a*-axis and *b*-axis; the azimuthal anisotropy decreases from 45.5% (0 GPa) to 29.81% (25 GPa). Ultimately, we have ascertained the lateral variations of the heat flow and discovered that heat flow increases with depth. These findings provide a robust foundation for furthering our understanding of the heat flow and temperature distribution in the Earth's interior.

ACKNOWLEDGMENTS

This work was supported by the National Natural Science Foundation of China (Nos. 41474067, 12174352). The use of the computational resources of the China University of Geosciences (Wuhan) is also acknowledged.

Supplementary Materials

There are several figures and tables that provided supporting information to the section of "Calculational Details" in the main text.

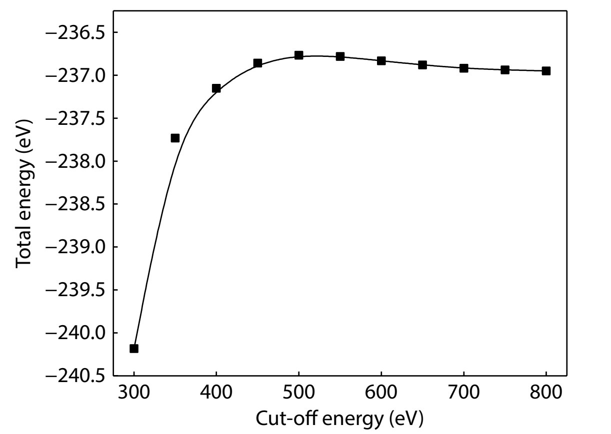

Figure S1. Relationship between total energy as a function of cut-off energy.

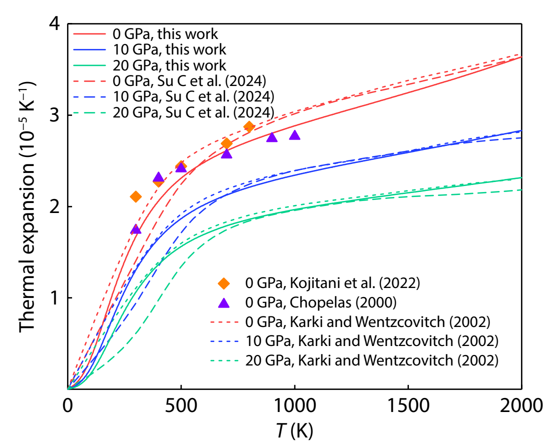

Figure S2. Temperature (*T*) dependence of thermal expansion (*α*) of $MgSiO_3$ akimotoite.

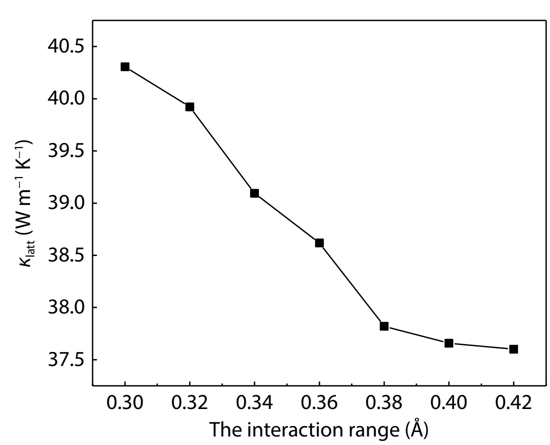

Figure S3. κ_{latt} of $MgSiO_3$ akimotoite with respect to the cutoff radius for anharmonic interaction.

Table S1. Calculated κ_{latt} with different q-point meshes at 25 GPa and 300 K.

	q-point meshes	κ_{latt} (W m^{-1} K^{-1})
$MgSiO_3$ akimotoite	11 × 11 × 5	37.61
	13 × 13 × 7	37.66
	15 × 15 × 9	38.09
MgPv	6 × 6 × 6	12.60
	8 × 8 × 8	13.46
	10 × 10 × 10	13.39

References

Blöchl, P. E. (1994). Projector augmented-wave method. *Phys. Rev. B*, *50*(24), 17953–17979. https://doi.org/10.1103/PhysRevB.50.17953

Carpenter, M. A., and Zhang, Z. Y. (2011). Anelasticity maps for acoustic dissipation associated with phase transitions in minerals. *Geophys. J. Int.*, *186*(1), 279–295. https://doi.org/10.1111/j.1365-246X.2011.05028.x

Chanyshev, A., Ishii, T., Bondar, D., Bhat, S., Kim, E. J., Farla, R., Nishida, K., Liu, Z. D., Wang, L., …Katsura, T. (2022). Depressed 660-km discontinuity caused by akimotoite–bridgmanite transition. *Nature*, *601*(7891), 69–73. https://doi.org/10.1038/s41586-021-04157-z

Chao, K. H., and Hsieh, W. P. (2019). Thermal conductivity anomaly in $(Fe_{0.78}Mg_{0.22})CO_3$ siderite across spin transition of iron. *J. Geophys. Res.: Solid Earth*, *124*(2), 1388–1396. https://doi.org/10.1029/2018JB017003

Chopelas, A. (2000). Thermal expansivity of mantle relevant magnesium silicates derived from vibrational spectroscopy at high pressure. *Am. Mineral.*, *85*(2), 270–278. https://doi.org/10.2138/am-2000-2-301

Cottaar, S., and Deuss, A. (2016). Large-scale mantle discontinuity topography beneath Europe: Signature of akimotoite in subducting slabs. *J. Geophys. Res.: Solid Earth*, *121*(1), 279–292. https://doi.org/10.1002/2015JB012452

Dekura, H., Tsuchiya, T., and Tsuchiya, J. (2013). *Ab initio* lattice thermal conductivity of $MgSiO_3$ perovskite as found in Earth's lower mantle. *Phys. Rev. Lett.*, *110*(2), 025904. https://doi.org/10.1103/PhysRevLett.110.025904

Dekura, H., and Tsuchiya, T. (2017). *Ab initio* lattice thermal conductivity of MgO from a complete solution of the linearized Boltzmann transport equation. *Phys. Rev. B*, *95*(18), 184303. https://doi.org/10.1103/PhysRevB.95.184303

Dekura, H., and Tsuchiya, T. (2019). Lattice thermal conductivity of $MgSiO_3$ Postperovskite under the lowermost mantle conditions from ab Initio anharmonic lattice dynamics. *Geophys. Res. Lett.*, *46*(22), 12919–12926. https://doi.org/10.1029/2019GL085273

Dziewonski, A. M., and Anderson, D. L. (1981). Preliminary reference Earth model. *Phys. Earth Planet. Inter.*, *25*(4), 297–356. https://doi.org/10.1016/0031-9201(81)90046-7

Ghaderi, N., Zhang, D. B., Zhang, H., Xian, J. W., Wentzcovitch, R. M., and Sun, T. (2017). Lattice thermal conductivity of $MgSiO_3$ perovskite from first principles. *Sci. Rep.*, *7*, 5417. https://doi.org/10.1038/s41598-017-05523-6

Guan, L. L., Yamazaki, D., Tsujino, N., Tange, Y., and Higo, Y. (2022). Seismic anisotropy in the lower mantle transition zone induced by lattice preferred orientation of akimotoite. *Geophys. Res. Lett.*, *49*(11), e2022GL098549. https://doi.org/10.1029/2022GL098549

Gubbins, D., Willis, A. P., and Sreenivasan, B. (2007). Correlation of Earth's magnetic field with lower mantle thermal and seismic structure. *Phys. Earth Planet. Inter.*, *162*(3-4), 256–260. https://doi.org/10.1016/j.pepi.2007.04.014

Haigis, V., Salanne, M., and Jahn, S. (2012). Thermal conductivity of MgO, $MgSiO_3$ perovskite and post-perovskite in the Earth's deep mantle. *Earth Planet. Sci. Lett.*, *355–356*, 102–108. https://doi.org/10.1016/j.epsl.2012.09.002

Hao, S. Q., Wang, W. Z., Qian, W. S., and Wu, Z. Q. (2019). Elasticity of akimotoite under the mantle conditions: Implications for multiple discontinuities and seismic anisotropies at the depth of ~600–750 km in subduction zones. *Earth Planet. Sci. Lett.*, *528*, 115830. https://doi.org/10.1016/j.epsl.2019.115830

He, J., Xu, M. J., Wu, Q. J., and Zhang, F. X. (2022). Hydrous melting driven upwelling from the mantle transition zone in the Mongolia Plateau revealed by receiver function analysis. *J. Geophys. Res.: Solid Earth*, *127*(11), e2022JB024905. https://doi.org/10.1029/2022JB024905

Hernández, E. R., Brodholt, J., and Alfè, D. (2015). Structural, vibrational and thermodynamic properties of Mg_2SiO_4 and $MgSiO_3$ minerals from first-principles simulations. *Phys. Earth Planet. Inter.*, *240*, 1–24. https://doi.org/10.1016/j.pepi.2014.10.007

Hofmeister, A. M. (2001). Thermal conductivity of spinels and olivines from vibrational spectroscopy: Ambient conditions. *Am. Mineral.*, *86*(10), 1188–1208. https://doi.org/10.2138/am-2001-1008

Hohenberg, P., and Kohn, W. (1964). Inhomogeneous electron gas. *Phys. Rev.*, *136*(3B), B864–B871. https://doi.org/10.1103/PhysRev.136.B864

Hsieh, W. P., Deschamps, F., Okuchi, T., and Lin, J. F. (2017). Reduced lattice thermal conductivity of Fe-bearing bridgmanite in Earth's deep mantle. *J. Geophys. Res.: Solid Earth*, *122*(7), 4900–4917. https://doi.org/10.1002/2017JB014339

Imada, S., Ohta, K., Yagi, T., Hirose, K., Yoshida, H., and Nagahara, H. (2014). Measurements of lattice thermal conductivity of MgO to core-mantle boundary pressures. *Geophys. Res. Lett.*, *41*(13), 4542–4547. https://doi.org/10.1002/2014GL060423

Ito, E., and Takahashi, E. (1989). Postspinel transformations in the system Mg_2SiO_4–Fe_2SiO_4 and some geophysical implications. *J. Geophys. Res.: Solid Earth*, *94*(B8), 10637–10646. https://doi.org/10.1029/JB094iB08p10637

Jackson, I. (1983). Some geophysical constraints on the chemical composition of the Earth's lower mantle. *Earth Planet. Sci. Lett.*, *62*(1), 91–103. https://doi.org/10.1016/0012-821X(83)90073-0

Karki, B. B., and Wentzcovitch, R. M. (2002). First-principles lattice dynamics and thermoelasticity of $MgSiO_3$ ilmenite at high pressure. *J. Geophys. Res.: Solid Earth*, *107*(B11), 2267. https://doi.org/10.1029/2001JB000702

Kawai, K., and Tsuchiya, T. (2009). Temperature profile in the lowermost mantle from seismological and mineral physics joint modeling. *Proc. Natl. Acad. Sci. USA*, *106*(52), 22119–22123. https://doi.org/10.1073/pnas.0905920106

Kennett, B. L. N., Engdahl, E. R., and Buland, R. (1995). Constraints on seismic velocities in the Earth from traveltimes. *Geophys. J. Int.*, *122*(1), 108–124. https://doi.org/10.1111/j.1365-246X.1995.tb03540.x

Kohn, W., and Sham, L. J. (1965). Self-consistent equations including exchange and correlation effects. *Phys. Rev.*, *140*(4A), A1133–A1138. https://doi.org/10.1103/PhysRev.140.A1133

Kojitani, H., Yamazaki, M., Tsunekawa, Y., Katsuragi, S., Noda, M., Inoue, T., Inaguma, Y., and Akaogi, M. (2022). Enthalpy, heat capacity and thermal expansivity measurements of $MgSiO_3$ akimotoite: Reassessment of its self-consistent thermodynamic data set. *Phys. Earth Planet. Inter.*, *333*, 106937. https://doi.org/10.1016/j.pepi.2022.106937

Kresse, G., and Furthmüller, J. (1996). Efficiency of ab-initio total energy calculations for metals and semiconductors using a plane-wave basis set. *Comp. Mater. Sci.*, *6*(1), 15–50. https://doi.org/10.1016/0927-0256(96)00008-0

Kresse, G., and Joubert, D. (1999). From ultrasoft pseudopotentials to the projector augmented-wave method. *Phys. Rev. B*, *59*(3), 1758–1775. https://doi.org/10.1103/PhysRevB.59.1758

Lay, T., Hernlund, J., and Buffett, B. A. (2008). Core–mantle boundary heat flow. *Nat. Geosci.*, *1*, 25–32. https://doi.org/10.1038/ngeo.2007.44

Li, L., Wentzcovitch, R. M., Weidner, D. J., and Da Silva, C. R. S. (2007). Vibrational and thermodynamic properties of forsterite at mantle conditions. *J. Geophys. Res.: Solid Earth*, *112*(B5), B05206. https://doi.org/10.1029/2006JB004546

Li, L., Weidner, D. J., Brodholt, J., Alfè, D., and Price, G. D. (2009). Ab initio molecular dynamics study of elasticity of akimotoite $MgSiO_3$ at mantle conditions. *Phys. Earth Planet. Inter.*, *173*(1-2), 115–120. https://doi.org/10.1016/j.pepi.2008.11.005

Li, W., Carrete, J., Katcho, N. A., and Mingo, N. (2014). ShengBTE: A solver of the Boltzmann transport equation for phonons. *Comput. Phys. Commun.*, *185*(6), 1747–1758. https://doi.org/10.1016/j.cpc.2014.02.015

Li, W., and Mingo, N. (2014). Lattice dynamics and thermal conductivity of skutterudites $CoSb_3$ and $IrSb_3$ from first principles: Why $IrSb_3$ is a better thermal conductor than $CoSb_3$. *Phys. Rev. B*, *90*(9), 094302. https://doi.org/

10.1103/PhysRevB.90.094302

Liang, T., Chen, W. Q., Hu, C. E., Chen, X. R., and Chen, Q. F. (2018). Lattice dynamics and thermal conductivity of lithium fluoride via first-principles calculations. *Solid State Commun.*, *272*, 28–32. https://doi.org/10.1016/j.ssc.2018.01.004

Liu, J., Wang, W., Yang, H., Wu, Z., Hu, M. Y., Zhao, J., Bi, W., Alp, E. E., Dauphas, N., … Lin, J. F. (2019). Carbon isotopic signatures of super-deep diamonds mediated by iron redox chemistry. *Geochem. Persp. Lett.*, *10*(10), 51–55. https://doi.org/10.7185/geochemlet.1915

Liu, M., and Yund, R. A. (1995). The elastic strain energy associated with the olivine-spinel transformation and its implications. *Phys. Earth Planet. Inter.*, *89*(3-4), 177–197. https://doi.org/10.1016/0031-9201(95)99098-E

Lu, C., and Chen, C. F. (2021). Indentation strengths of zirconium Diboride: Intrinsic versus extrinsic mechanisms. *J. Phys. Chem. Lett.*, *12*(11), 2848–2853. https://doi.org/10.1021/acs.jpclett.1c00434

Meng, Y., Weidner, D. J., Gwanmesia, G. D., Liebermann, R. C., Vaughan, M. T., Wang, Y., Leinenweber, K., Pacalo, R. E., Yeganeh-haeri, A., and Zhao, Y. (1993). In situ high P-T X ray diffraction studies on three polymorphs (α, β, γ) of Mg_2SiO_4. *J. Geophys. Res.: Solid Earth*, *98*(B12), 22199–22207. https://doi.org/10.1029/93JB02383

Monkhorst, H. J., and Pack, J. D. (1976). Special points for Brillouin-zone integrations. *Phys. Rev. B*, *13*(12), 5188–5192. https://doi.org/10.1103/PhysRevB.13.5188

Núñez-Valdez, M., da Silveira, P. and Wentzcovitch, R. M. (2011). Influence of iron on the elastic properties of wadsleyite and ringwoodite. *J. Geophys. Res.: Solid Earth*, *116*(B12), B12207. https://doi.org/10.1029/2011JB008378

Núñez-Valdez, M., Wu, Z. Q., Yu, Y. G., Revenaugh, J., and Wentzcovitch, R. M. (2012). Thermoelastic properties of ringwoodite $(Fe_x, Mg_{1-x})_2SiO_4$: Its relationship to the 520 km seismic discontinuity. *Earth Planet. Sci. Lett*, *351–352*, 115–122. https://doi.org/10.1016/j.epsl.2012.07.024

Núñez-Valdez, M., Wu, Z., Yu, Y. G., and Wentzcovitch, R. M. (2013). Thermal elasticity of $(Fe_x, Mg_{1-x})_2SiO_4$ olivine and wadsleyite. *Geophys. Res. Lett.*, *40*(2), 290–294. https://doi.org/10.1002/grl.50131

Ohta, K., Yagi, T., Taketoshi, N., Hirose, K., Komabayashi, T., Baba, T., Ohishi, Y., and Hernlund, J. (2012). Lattice thermal conductivity of $MgSiO_3$ perovskite and post-perovskite at the core–mantle boundary. *Earth Planet. Sci. Lett.*, *349–350*, 109–115. https://doi.org/10.1016/j.epsl.2012.06.043

Ohta, K., Yagi, T., Hirose, K., and Ohishi, Y. (2017). Thermal conductivity of ferropericlase in the Earth's lower mantle. *Earth Planet. Sci. Lett.*, *465*, 29–37. https://doi.org/10.1016/j.epsl.2017.02.030

Okuda, Y., Ohta, K., Sinmyo, R., Hirose, K., Yagi, T., and Ohishi, Y. (2019). Effect of spin transition of iron on the thermal conductivity of (Fe, Al)-bearing bridgmanite. *Earth Planet. Sci. Lett.*, *520*, 188–198. https://doi.org/10.1016/j.epsl.2019.05.042

Osako, M., Ito, E., and Yoneda, A. (2004). Simultaneous measurements of thermal conductivity and thermal diffusivity for garnet and olivine under high pressure. *Phys. Earth Planet. Inter.*, *143–144*, 311–320. https://doi.org/10.1016/j.pepi.2003.10.010

Ouyang, Y. L., Yu, C. Q., He, J., Jiang, P. F., Ren, W. J., and Chen, J. (2022). Accurate description of high-order phonon anharmonicity and lattice thermal conductivity from molecular dynamics simulations with machine learning potential. *Phys. Rev. B*, *105*(11), 115202. https://doi.org/10.1103/PhysRevB.105.115202

Pertermann, M., and Hofmeister, A. M. (2006). Thermal diffusivity of olivine-group minerals at high temperature. *Am. Mineral.*, *91*(11-12), 1747–1760. https://doi.org/10.2138/am.2006.2105

Ringwood, A. E. (1975). *Composition and Petrology of the Earth's Mantle*. New York: McGraw-Hill.

Siersch, N. C., Kurnosov, A., Criniti, G., Ishii, T., Boffa Ballaran, T., and Frost, D. J. (2021). The elastic properties and anisotropic behavior of $MgSiO_3$ akimotoite at transition zone pressures. *Phys. Earth Planet. Inter.*, *320*, 106786. https://doi.org/10.1016/j.pepi.2021.106786

Su, C., Song, W., Yang, G., Liu, Y. G., and Li, Q. Y. (2024). Pressure effects on the thermodynamic properties of $MgSiO_3$ akimotoite. *Crystals*, *14*(10), 837. https://doi.org/10.3390/cryst14100837

Suzuki, I., Ohtani, E., and Kumazawa, M. (1979a). Thermal expansion of γ-Mg_2SiO_4. *J. Phys. Earth*, *27*(1), 53–61. https://doi.org/10.4294/jpe1952.27.53

Suzuki, I., Ohtani, E., and Kumazawa, M. (1980b). Thermal expansion of modified spinel, β-Mg_2SiO_4. *J. Phys. Earth*, *28*(3), 273–280. https://doi.org/10.4294/jpe1952.28.273

Tauzin, B., Debayle, E., and Wittlinger, G. (2008). The mantle transition zone as seen by global *Pds* phases: No clear evidence for a thin transition zone beneath hotspots. *J. Geophys. Res.: Solid Earth*, *113*(B8), B08309. https://doi.org/10.1029/2007JB005364

Togo, A., and Tanaka, I. (2015). First principles phonon calculations in materials science. *Scripta Mater.*, *108*, 1–5. https://doi.org/10.1016/j.scriptamat.2015.07.021

Wang, D., Wu, Z. Q., and Deng, X. (2023). Thermal conductivity of Fe-bearing bridgmanite and post-perovskite: Implications for the heat flux from the core. *Earth Planet. Sci. Lett.*, *621*, 118368. https://doi.org/10.1016/j.epsl.2023.118368

Wang, Y. B., Uchida, T., Zhang, J. Z., Rivers, M. L., and Sutton, S. R. (2004). Thermal equation of state of akimotoite $MgSiO_3$ and effects of the akimotoite–garnet transformation on seismic structure near the 660 km discontinuity. *Phys. Earth Planet. Inter.*, *143–144*, 57–80. https://doi.org/10.1016/j.pepi.2003.08.007

Weidner, D. J., and Ito, E. (1985). Elasticity of $MgSiO_3$ in the ilmenite phase. *Phys. Earth Planet. Inter.*, *40*(1), 65–70. https://doi.org/10.1016/0031-9201(85)90006-8

Weidner, D. J., and Li, L. (2010). Impact of phase transitions on p wave velocities. *Phys. Earth Planet. Inter.*, *180*(3-4), 189–194. https://doi.org/10.1016/j.pepi.2009.11.006

Xu, Y. S., Shankland, T. J., Linhardt, S., Rubie, D. C., Langenhorst, F., and Klasinski, K. (2004). Thermal diffusivity and conductivity of olivine, wadsleyite and ringwoodite to 20 GPa and 1373 K. *Phys. Earth Planet. Inter.*, *143–144*, 321–336. https://doi.org/10.1016/j.pepi.2004.03.005

Yang, D. P., Wang, W. Z., and Wu, Z. Q. (2017). Elasticity of superhydrous phase B at the mantle temperatures and pressures: Implications for 800 km discontinuity and water flow into the lower mantle. *J. Geophys. Res.: Solid Earth*, *122*(7), 5026–5037. https://doi.org/10.1002/2017JB014319

Yang, S., Dong, W. X., Zhang, L., He, K. H., Dai, W., and Lu, C. (2023). Lattice thermal conductivity of Mg_2SiO_4 olivine and its polymorphs under extreme conditions. *Phys. Chem. Miner.*, *50*(2), 16. https://doi.org/10.1007/s00269-023-01240-x

Yu, Y. G., Wentzcovitch, R. M., Vinograd, V. L., and Angel, R. J. (2011). Thermodynamic properties of $MgSiO_3$ majorite and phase transitions near 660 km depth in $MgSiO_3$ and Mg_2SiO_4: A first principles study. *J. Geophys. Res.: Solid Earth*, *116*(B2), B02208. https://doi.org/10.1029/2010JB007912

Zhang, Y. G., Zhao, D. P., and Matsui, M. (2005). Anisotropy of akimotoite: A molecular dynamics study. *Phys. Earth Planet. Inter.*, *151*(3-4), 309–319. https://doi.org/10.1016/j.pepi.2005.04.003

Zhang, Z., and Wentzcovitch, R. M. (2021). *Ab initio* lattice thermal conductivity of $MgSiO_3$ across the perovskite-postperovskite phase transition. *Phys. Rev. B*, *103*(14), 144103. https://doi.org/10.1103/PhysRevB.103.144103

Zhao, Y. J., Wu, Z. Q., Hao, S. Q., Wang, W. Z., Deng, X., and Song, J. (2022). Elastic properties of Fe-bearing Akimotoite at mantle conditions: Implications for composition and temperature in lower mantle transition zone. *Fundam. Res.*, *2*(4), 570–577. https://doi.org/10.1016/j.fmre.2021.12.013